



Fabrication of sub-20nm nano-gap structures through the elastomeric nano-stamp assisted secondary sputtering phenomenon.

Journal:	<i>Nanoscale</i>
Manuscript ID:	NR-ART-11-2013-006346.R1
Article Type:	Paper
Date Submitted by the Author:	04-Mar-2014
Complete List of Authors:	Jeon, Hwan-Jin; Korea Advanced Institute of Science and Technology, Department of Chemical + Biomolecular Engineering Lee, Eun Hyeong; Korea Advanced Institute of Science and Technology, Department of Chemical and Biomolecular Engineering Yoo, Hae-Wook; Korea Advanced Institute of Science and Technology, Department of Chemical and Biomolecular Engineering Kim, Kyong Hwan; Korea Advanced Institute of Science and Technology, Department of Chemical + Biomolecular Engineering Jung, Hee-Tae; Korea Advanced Institute of Science and Technology, Department of Chemical + Biomolecular Engineering

Fabrication of sub-20nm nano-gap structures through the elastomeric nano-stamp assisted secondary sputtering phenomenon

Hwan-Jin Jeon[†], Eun Hyeong Lee[†], Hae-Wook Yoo, Kyoung Hwan Kim and Hee-Tae Jung^{1, *}

Received (in XXX, XXX) Xth XXXXXXXX 20XX, Accepted Xth XXXXXXXX 20XX

First published on the web Xth XXXXXXXX 20XX

DOI: 10.1039/b000000x

We describe a highly efficient method for fabricating a controllable and reliable sub-20nm scale nano-gap structures through an elastomeric nano-stamp with an embedded ultra-thin pattern. The metals embedded in the stamp consist of ultrahigh resolution (approximately 10 nm) and high aspect ratio (ca. 15) nano-structures, which are based on secondary sputtering lithography (SSL). The nano-gap structures fabricated in this fashion achieve a high resolution and meet the requirements of minimal cost, high reliability, controllability, reproducibility, and applicability to different materials. Further, we demonstrate that this method enables the fabrication of SERS substrates for detection at the single-molecule level.

15 Introduction

Fabrication of nano-gap structures with tens of nano-meters spacing between highly periodic nano-structures have recently received significant attention. Recently, single-molecule and nanotube/wire based electronic devices using nano-gap electrodes have unique merits such as efficient power dissipation, self-assembly properties and lower fabrication costs¹⁻⁸. In particular patterning of nano-gap structures with highly uniformity and precision enables the increases of reproducibility, sensitivity, and long-term stability of devices¹⁻⁴. The nano-gap patterned structures can lead to a significant level of integration with lower power consumption, higher performance and lower fabrication costs in electronic applications⁵⁻⁸. In addition, nano-gap patterned structures can generate an enhanced electromagnetic field through surface plasmons in a narrow gap. This is a significant challenge for a variety of plasmonic applications such as surface plasmon enhanced fluorescence and surface enhanced Raman spectroscopy⁹⁻¹⁴. Several advanced nano-gap patterning techniques including mask-assisted¹⁵, colloid assembly¹⁶⁻¹⁷, angle-deposited¹⁸, block copolymer¹⁹⁻²⁰ and edge lithography²¹, have been suggested in order to meet the requirements of superior nano-gap patterned structures with uniformity and large scale reproducibility. In spite of the intensive effort in this field, these lithography techniques suffer from their inability to achieve ultrahigh resolution on the order of approximately 10 nm gaps while maintaining a simple fabrication process. Although

alternative advanced methods have been suggested in recent years, it is still an on-going challenge to fabricate reliable and controllable nano-gap patterned structures with very large surface areas.

We recently reported a new patterning method known as “secondary sputtering lithography”²²⁻²⁴, which was seen to be a new concept for 3-dimensional lithography that can fabricate sub-20 nm scale 3D patterned nano-structures with a high aspect ratio over a large area through an effective fabrication process. This innovative patterning method utilizes the secondary sputtering phenomenon, which is the angular distribution of target material particles generated through an ion-bombardment process. Due to the single step, the emitted target particles generated by the secondary sputtering phenomenon are absorbed physically onto the pre-pattern which is made using conventional lithography methods. A sub-20 nm scale 3-dimensional (3D) nano-pattern that corresponds to the 3D shape of the pre-pattern is created with high uniformity and accuracy.

In the remainder of this paper, we present a modification to the secondary sputtering approach to fabricate sub-20 nm scale nano-gap structures through the elastomeric nano-stamp method using an ultrathin metal pattern embedded elastomeric PDMS mold. The metals embedded in the stamp consist of ultrahigh resolution (approximately 10 nm) and high aspect ratio (ca. 15) nano-structures, which are based on secondary sputtering lithography (SSL). Using the sub-20 nm scale patterned structures with a high aspect ratio as a stamp, sub-20 nm scale nano-gap structures with

a negative copy of the pattern stamp can be fabricated over large surface areas. The nano-gap structures fabricated in this fashion achieve a high resolution and meet the requirements of minimal cost, high reliability, controllability, reproducibility and applicability to different materials. Further, we demonstrate that this method enables the fabrication of SERS substrates for detection at the single-molecule level.

Experimental

Various patterns were fabricated by secondary sputtering lithography (SSL). For fabrication of sub-20 nm scale metal patterns, firstly the wafers are treated by Piranha solution to clean the surface (it should be noted that Piranha attacks organics). The Piranha solution was prepared by mixing sulfuric acid (H_2SO_4 96 %) and hydrogen peroxide (H_2O_2 30 %) at a 3:1 volume ratio. The fragment of silicon wafers was immersed into the solution for approximately 10 - 15 min. The wafers were then rinsed with DI water and blown with nitrogen. After the cleaning was complete, the sample was exposed to oxygen plasma treatment (100 W, 75 Pa) to increase adhesion between PEDOT:PSS (Clevios, PH500) and the wafers. And then PEDOT:PSS was spin-coated at 4,000 rpm for 25 s on the silicon wafers as a water soluble layer. 20nm thickness PEDOT:PSS film was fabricated after thermal baking process (120 °C, 5 min). The highly uniform platinum was deposited on the prepared substrate using e-beam evaporation (approximately 40 nm thick). A polystyrene [PS (18,000 g/mol), Sigma-Aldrich] / toluene (anhydrous 99.8%, Sigma-Aldrich) solution (4 wt%) was spin-coated at 3,000 rpm for 45 s on the substrate to fabricate a thin PS film (120 nm thickness).

Line-space patterned silicon with 500 nm width/spacing was prepared with e-beam lithography. The fabrication of replica pattern, hard PDMS was prepared by mixing trimethyl siloxy-terminated vinyl methyl siloxane-dimethyl siloxane copolymers (Gelest Inc., 3.4g), 2,4,6,8-tetramethyl tetra vinyl cyclo tetra siloxane (Sigma-Aldrich, 18 μl), Pt-divinyl tetra methyl siloxane, trimethyl siloxy-terminated methyl hydrosiloxane (Gelest Inc., 18 μl), and dimethyl siloxane copolymers (JSI silicon, 1g)²⁶. This hard PDMS mixture was immediately spin-coated onto the

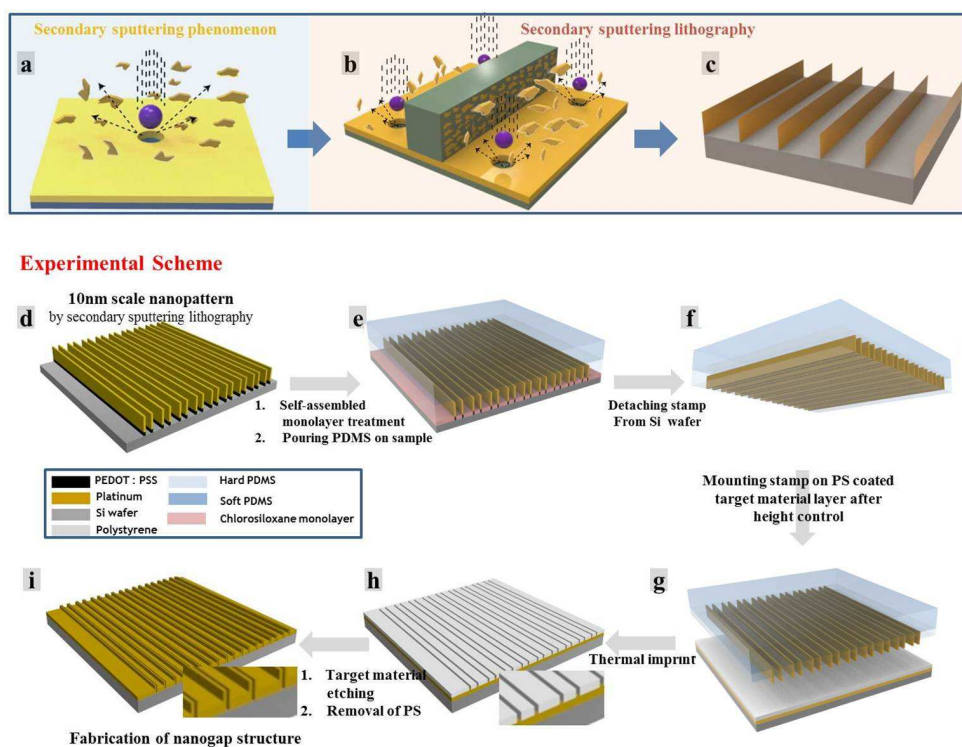


Figure 1. Schematic presentation of the fabrication of a nano-gap structure using an elastomeric stamp with an embedded ultrathin pattern. a-c) Representative images of the secondary sputtering phenomenon and secondary sputtering lithography (SSL) technique. d) Fabrication of ultra-high resolution (approximately 10 nm) patterns with a high aspect ratio on the PEDOT:PSS coated Pt substrates using secondary sputtering lithography. e) Fabrication of the elastomeric PDMS body on a patterned substrate through the curing of h-PDMS and s-PDMS. f) Detachment of only the elastomeric stamp with an embedded nano-pattern from wafer substrate by ultra-sonication in DI water. g-h) Fabrication of a nano-gap pattern of a PS layer using a nano-stamp with an embedded nano-pattern. i) The patterned nano-gap structure of the target material fabricated by the etching process.

patterned silicon master at 1,500 rpm for 25 s and pre-cured for 10 min at 60 °C. Then, soft PDMS was prepared by pouring the mixture of PDMS prepolymer (Sylgard 184 A:B -10:1, Dow Corning) onto the hard PDMS layer and curing at 80 °C for 2 h. This cured PDMS mold with topographic features was placed onto the PS coated film. The various PS patterns were fabricated when each shape of the PDMS molds were mounted on the PS surface and heated at 135 °C for 40 min in vacuum oven. The residual PS layer was removed by an O_2/CF_4 RIE process at a flow of 40/60 sccm and a chamber pressure of 20 mTorr. The RF power was 80 W. After low energy Ar^+ ion milling (500 eV, VTS corporation), platinum pattern (width of approximately 15 nm, height of approximately 200 nm) was produced using secondary sputtering lithography (Fig. 1a-1c). The remaining polymer resist was then removed through the O_2 RIE process, and the bottom of the metal patterns was etched during the second ion milling process (Fig. 1d).

In this paragraph, the preparation of the metal embedded stamp is described (Fig. 1d-1i). The sub-20nm scale line pattern by SSL method acted as a stamp tip and new PDMS acted as stamp body (Fig. 1e, 1f). A metal patterned substrate was placed on a

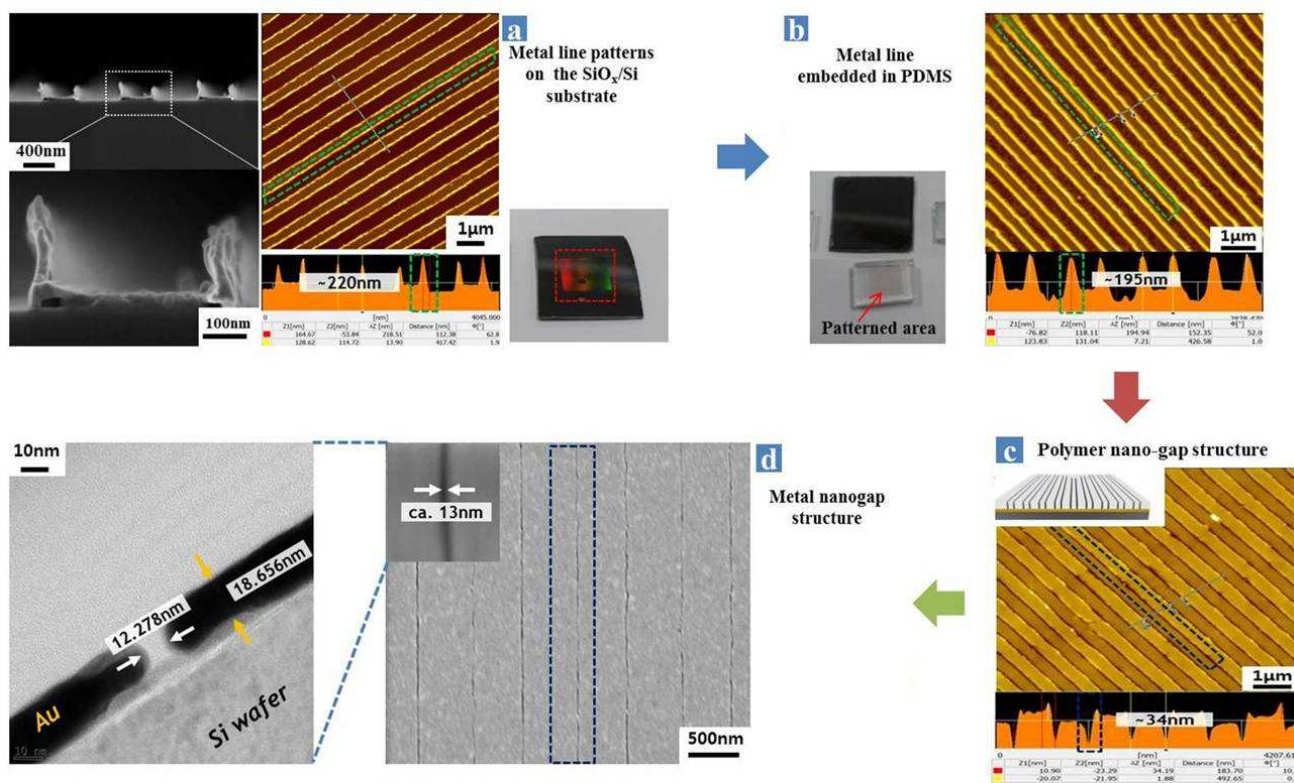


Figure 2. AFM, SEM, TEM and photo images that support the representative process for nano-gap fabrication (a – d). a) Pt line patterns with 15 to 17 nm width, 220 nm height and 500 nm period fabricated by secondary sputtering lithography. b) AFM and photo images for elastomeric PDMS stamp with embedded Pt line patterns. c) AFM image for PS line gap patterns on Au substrate after the stamping process. d) SEM and TEM images for Au line gap patterns with approximately 13 nm width, approximately 20 nm thickness, 500 nm period and 5 mm x 5 mm area. Green dashed lines show the Pt line pattern, while the blue dashed lines show the trenced area.

desiccator that contained trichloromethylsilane (15 μ L) to coat the siloxane monolayer on SiO_x. After 30 minutes under vacuum, the patterned samples were spin-coated with h-PDMS through same mixing steps as explained above. The sample was then cooled and dipped in DI water under ultra-sonication to detach the metal embedded stamp from the SiO_x/Si wafer while PEDOT:PSS (water soluble polymer) was dissolved in the water. The stamp was then dried under a nitrogen stream and carefully stripped off. The remained PEDOT:PSS residues were washed by rinsing with acetone/water and the blunt terminal of platinum protrusions were etched by additional ion-milling process. Since the height of platinum protrusions embedded in PDMS stamps was not enough to stamping, this height was controlled by etching the PDMS surface using the fluorine based RIE process at a flow rate of 25/75 sccm (20 mTorr, RF power of 203 W).

In this paragraph we describe the nano-gap structure fabrication through the metal embedded stamp (Fig. 1g-1i). A highly uniform gold layer (approximately 20 nm) / Cr layer (adhesion layer of 1.5 nm) was deposited by e-beam evaporation onto silicon wafers (Fig. 1g). It is important to note that different types of metal nano-gap structures can be prepared by depositing other metals onto a substrate with Cr adhesion layer. This sample was spin-coated with a PS (18,000 g/mol) polymer resist. The metal embedded stamp was then placed onto the PS coated substrate, and air bubbles of composite samples were removed

under vacuum (Fig. 1h). A moderate pressure (approximately 200 g/cm²) and heat above the glass transition temperature (135 $^{\circ}$ C) of the polymer resist was applied onto the top of the stamp for 30 minutes. After cooling at room temperature, the stamp was carefully peeled from the surface. Then the polystyrene layer with indentations replicating the protruding line pattern from metal embedded stamp is obtained. Nano sized grooved PS coated gold layer was etched through ion-milling process by using the PS layer as mask, until the metal layer is removed at the bottom of the PS trenches. The remaining polymer on the noble metals was cleaned using the O₂ RIE process (Fig. 1i).

In this paragraph we describe the Surface-enhanced Raman Scattering (SERS). To examine the SERS activity, BCB (Brilliant Cresyl Blue) solution (20 μ l of a 1.0 x 10⁻⁵ M solution in ethanol) was drop-casted to the sample. After complete drying of the solution in the desiccator for 3 hours, the sample was blown with nitrogen and the remaining single molecules were disposed by rinsing with clean ethanol. The SERS spectra from the nano-gap structures were measured through a high resolution dispersive Raman spectroscope (LabRAM HR UV/vis/NIR, Horiba Jobin Yvon) based on a high stability BXFM confocal microscope. The VIS 632.8 nm radiation of a He-Ne laser was prepared and focused on the sample using the 100 x objective. The Raman signal was recorded with a multi-channel thermoelectric cooled (-70 $^{\circ}$ C) CCD detector mounted on the spectrometer with a 600

mm⁻¹ groove grating, resulting in a spectral resolution of 1 cm⁻¹. The SERS intensity data of various structures was selected at 5 random points that showed a strong signal, since it is difficult to observe the intersecting point of a line gap using only the optical microscope.

In this section we describe the SERS enhancement factor (EF) calculations. The EF was calculated at a shift of approximately 583 cm⁻¹ of the surfaced-adsorbed BCB, which is the largest peak. The EF is defined by

$$EF = \frac{I_{SERS} \times N_{bulk}}{I_{bulk} \times N_{SERS}}$$

where I_{SERS} is the Raman intensity of the 583 cm⁻¹ peak on patterned Au substrates and I_{bulk} is the Raman signal of the same band on a Si substrate. N_{SERS} and N_{bulk} are the number of molecules on the illuminated area (radius = 500 nm) and are proportional to the effective surface area of the pattern, which subtracts the area in the nano-gap and includes the area of the side wall of the nano-structures.

In this paragraph we describe the surface topological measurement.

The surface topological measurements were performed under ambient conditions with a commercial AFM (SPA400; Seiko, Japan), equipped with a 100 × 100 μm² scan head. All substrates were imaged in non-contact mode using standard Si₃N₄ cantilevers with a nominal spring constant of 0.08 N m⁻¹. SEM (S-4800; Hitachi, Japan, sirion FE-SEM and Magellan400; FEI, USA) images were obtained by collecting the secondary electrons produced by bombarding the sample with an incident electron beam of 1 to 10 kV.

Results and Discussion

In Figure 2 the representative atomic force microscope (AFM), scanning electron microscope (SEM) and transmission electron microscope (TEM) images of the patterned structures at each fabrication steps are shown. Platinum line patterns (w =

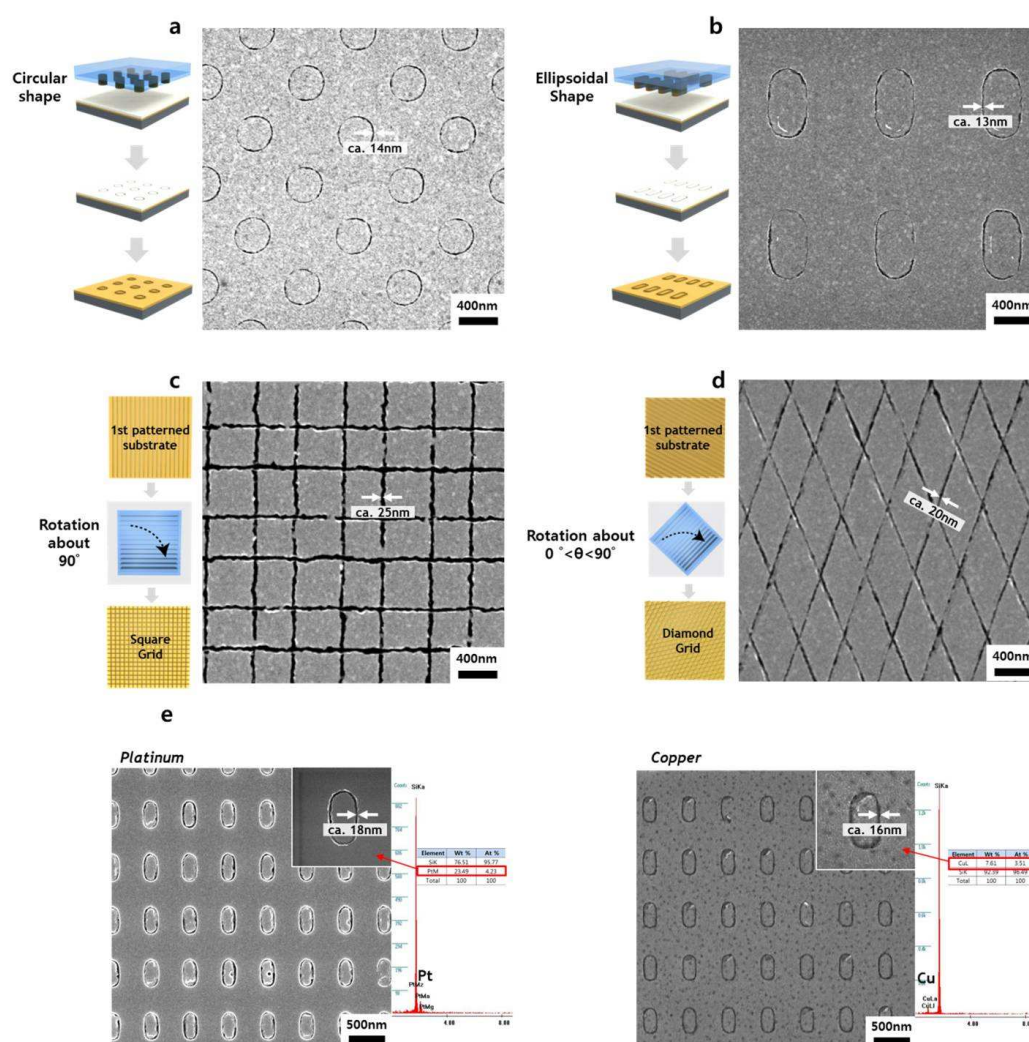


Figure 3. SEM images and corresponding schematic illustrations for various nano-gap structures (a-d) and ellipsoidal nano-gap pattern for various materials (e). a-b) Circular shape (approximately 14 nm) and ellipsoidal shape (approximately 13 nm) of nano-gap structures using the nano-stamp to embed circular and ellipsoidal hole-cylinder Pt patterns, respectively. c-d) Fabrication of the grid nano-gap pattern of squares (approximately 25 nm) and diamonds (approximately 20 nm) by multiple imprinting with an angle variation of 90° and 0° < θ < 90° with respect to first patterned substrate. e) Ellipsoidal shaped nano-gap pattern of various materials (Pt, Cu).

approximately 15, s = 500 nm, h = 200 nm) were generated on the silicon wafer substrate over a large area (5 mm X 5 mm) via the secondary sputtering lithography (Fig. 2a). In Figure 2b the elastomeric PDMS stamp with an embedded platinum line pattern after the pattern transfer process step into the PDMS body and post RIE process are shown. The protruding platinum line pattern on the PDMS body has a center-to-center spacing of 500 nm and a height of approximately 195 nm, which is almost within the feature dimensions of the original Pt pattern on the silicon wafer (Fig. 2b). It is worth mentioning that the h-PDMS is based on vinyl and hydrosilane end-lined polymers with a higher Young modulus (~9 N/mm²) that help to hold the metal structures in comparison to sylgard 184 soft PDMS (~2 N/mm²). It is vital that the non-trenched area acts as a mask area to protect the target metal layer during the etching process of the gold layer for the transfer process of the polymer pattern to the metal substrate to

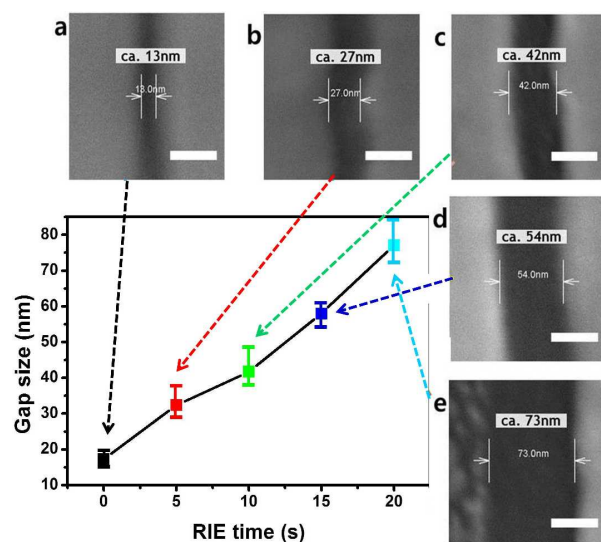


Figure 4. Plot showing the relation between the gap size of Au nano-structures and oxygen based reactive ion etching time. The width of the gap between Au nano-structures is increased with proportion to the RIE time. The initial width of the gap before isotropic RIE was 13 nm (a). After isotropic RIE at 5, 10, 15, and 20 seconds, the gap size became 27, 42, 54 and 73 nm, respectively (b – e). Scale bar 40 nm.

succeed. After the printing of the elastomeric nano-stamp onto the PS polymer layer, the sub-20 nm scale nano-gap pattern of the PS polymer layer was fabricated with uniformity (Fig. 2c). Through the ion-milling process and RIE process, the approximate 10 nm scale nano-gap structured pattern of target materials was fabricated with uniformity over the large surface areas (Fig. 2d). To further confirm that the sub-20 nm scale gap nano-structure was fabricated successfully, we performed cross-sectional TEM analysis by cutting the center of the nano-gap substrate perpendicular to the gap direction (Fig. 2d). The TEM results show that the height difference between the trenched and non-trenched area was approximately 20 nm, whereas the nano-gap size and width are 12.278 nm and 500 nm, respectively, confirming that our elastomeric stamp embedded Pt line pattern by secondary sputtering lithography can achieve the effective fabrication of sub-20 nm scale nano-gap patterned structures. In addition, the trenched area between the nano-structures only revealed a Si component while nano-structures showed Au peaks in the EDX spectroscopy, indicating that the Au of the gap regions were clearly fabricated through the ion-milling process (the supporting information is in Figure S1).

Various nano-gap structures with different shapes / materials can be prepared through the application of a different elastomeric nano-stamp that includes a variety of sub-20 nm scale nano-gap

patterns with different shapes and dimensions (Fig. 3). Figure 3a, 3b show the circular shaped gap patterns with approximately 15 nm gap size and 400 nm diameter with an ellipsoidal shaped gap pattern with approximately 15 nm gap size and 800 nm – 400 nm diameter, respectively. It is worth mentioning that our method using the nano-stamp can be utilized several times on the same substrate, resulting in complex sub-20 nm scale nano-gap patterns. This means that a single nano-stamp made from a corresponding single master pattern can generate various nano-gap structures. The grid pattern of the square shape, second stamping with an angle of 90 degrees, was also fabricated. The resulting gap structured pattern has a length (l) of period 500 nm and a gap (g) of 25 nm (Fig. 3c). It is also important that the metal embedded stamp retains its original topography without critical damages during repeated stamping. (Supporting Information S3). Similarly, the grid pattern of the diamond shape can be fabricated through rotation of the metal embedded stamp from 0° to 90° with respect to the first patterned substrate (Fig. 3d). More complex nano-structures can be prepared by altering the rotation of the metal embedded stamp and imprinting several times. In addition, this method can also be applied to various materials. Ellipsoidal shaped nano-gap patterns with platinum and copper could be fabricated using the same technique (Fig. 3e). We have found from our experimental results so far, that most materials can be fabricated in the nano-gap structure using this technique.

We found that the feature size of the nano-gap can be controlled by varying the RIE processing condition. An oxygen based RIE process is a purely chemical etching where free radicals react with the polymer and form a volatile gas product. In fact, the presence of O₂ in the RIE process increases the isotropic etching rate for the PS polymer resists in a low vacuum state²⁵. This phenomenon can be utilized to etch the side surface of the PS pattern. It is expected that the gap size between the stamped polymer patterns will increase with the RIE time. As a result, the width of the nano-gap structure increases as the RIE etching time of the polymer structure increases. Initially, the gap size between the nano-structures was 13 nm without the RIE etching (Fig. 4a). Increasing the RIE time from 5 s to 10 s, 15 s, and 20 s, the gap size linearly increased to 27 nm, 42 nm, 54 nm, and 73 nm, respectively (Fig. 4b-4e). However, when the etching time exceeded 15s, over-etching of the gold layer was observed (Fig. 4e). Since the reactive ion-etching removes the PS patterns entirely, small PS layers rarely existed after the 20 s RIE etching process. The resulting gold layer was not covered with PS and is etched by the gold etching process. However, this problem can be resolved by simply increasing both the thickness of the polymer resist and the height of the prominent metal patterns in the stamp.

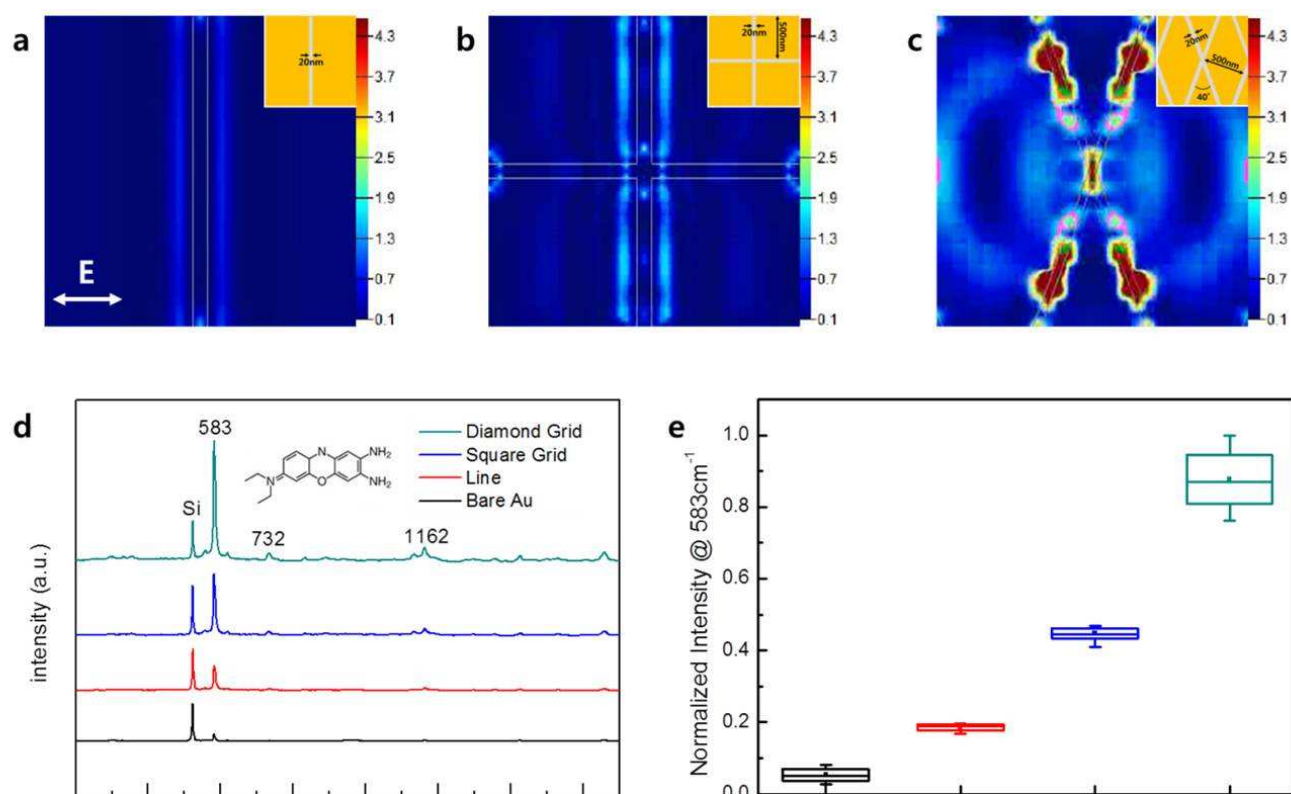


Figure 5. FDTD simulations and SERS spectra of BCB by focusing the light of a 632.8 nm He-Ne laser on various nano-gap structures. The result of the FDTD simulations revealed that the grid pattern of the diamond was approximately 2.64 and 3.80 times stronger than that of the squared grid and line: (a) line; (b) squared grid; (c) diamond grid; inset: color bar showing the level of the electromagnetic fields. SERS spectra according to various shapes showed distinguishable peaks around 583 cm^{-1} , 732 cm^{-1} and 1162 cm^{-1} (d). Comparison of the normalized intensity at 583 cm^{-1} according to various shapes revealed that the average intensity of the diamond grid was approximately 1.96, 4.74 and 16.5 times stronger than that of the squared grid, line, and bare Au, respectively (e).

To demonstrate the novelty of our approach for high resolution nano-gap structures, we examined surface-enhanced Raman scattering (SERS) in the presence of various nano-gap structures, which have been widely studied based on interesting optical properties from nano-scale structures of metals. The nano-gap patterns fabricated through the elastomeric nano-stamp have the potential to act as a SERS substrate due to their unique peculiarities for ultra-narrow gap and structural effects, which is favorable for the formation of plasmonic environments¹⁵. The narrow gap between metallic structures is essential for the effective generation of localized surface plasmon resonance (LSPR). This is due to the hot spot phenomenon which can cause collective resonance for SPR from the narrow gap¹⁵⁻¹⁷. Therefore, it is expected that our patterned sub-20 nm scale gap structures can achieve the sensitivity, reproducibility, and long-term stability for SERS based sensing devices. In order to demonstrate this, an initial attempt was performed by examining the electromagnetic field generation near the nano-gap structures via a FDTD simulation. The FDTD simulations were performed with commercial software (Lumerical Solutions Inc., FDTD Solutions 8.0). For effective simulation results, the adhesion layer of the chromium was omitted and only a small fraction of the total area was simulated due to a periodic nano-structure about the planar dimension. The dielectric constants of the various metals were selected from the software's chemical database. The simulated

models were designed for line (Fig. 5a), squared grid (Fig. 5b) and diamond-shaped grids (Fig. 5c), in order to identify the electromagnetic field generation on the different nano-gap configurations. The sharp-edged structural pattern is expected to lead to much higher electromagnetic fields, typically called the 'lightening rod effect', as well as multi-polar plasmon resonance due to their anisotropic shape. The wavelength of the incident electromagnetic source was 633 nm which was the excitation wavelength of the SERS molecules. (Supporting Information is in S5 for further FDTD simulation results). The FDTD simulation of the line gap shows the amplification of the electromagnetic field (Fig. 5a), while the simulation of the square grid gap pattern shows a strong electromagnetic field in the gap compared to the line gap patterns (Fig. 5b). Further, the diamond shaped gap pattern with a sharp tip has a stronger electromagnetic field in relation to the square grid (Fig. 5c). As a result, the FDTD simulation results show that the electromagnetic field of the diamond grid patterns was approximately 2.64 and 3.80 times stronger than those of the squared grid and line patterns.

We found that the shape of the nano-gap metal structure strongly affects the SERS performance sensitivity, which was in agreement with our FDTD simulation results (Fig. 5). The SERS spectra results of the solution (Fig. 5d) show that a large peak around 583 cm^{-1} was presented, with recognizable peaks around 732 cm^{-1} and 1162 cm^{-1} . These additional peaks are also present

in previous results of brilliant cresyl blue (BCB) spectra²⁹. In addition, the intensity of each peak (averaged value of 5 random points) in the nano-gap patterned Au substrates is much larger than a bare Au substrate even with the same concentration of solution. Thus, the region of the nano-gap patterns plays a crucial role for enhancing the sensitivity of SERS induced by LSPR. The normalized intensity of the 583 cm⁻¹ peak for various nano-gap structures is shown, where the value is calculated by selecting 5 random points (Fig. 5e). The average intensity of the diamond grid was approximately 1.96, 4.74, and 16.5 times stronger than those of the square grid, line and bare Au, respectively. Specifically, the SERS enhancement factor (EF) value of the diamond grid structure with a sharp edge is 3.74×10⁵, by evaluating the maximum intensities of the Raman signal at a shift of 583 cm⁻¹. EF is defined by $EF = (I_{SERS} \times N_{bulk}) / (I_{bulk} \times N_{SERS})$, where I_{SERS} is the Raman intensity of the 583 cm⁻¹ band resulting from BCB molecules on the patterned nano-gap structures and I_{bulk} is the Raman signal of the same band on a bare Si substrate. N_{SERS} and N_{bulk} are the number of molecules on the illuminated area and are proportional to the effective surface area of the pattern.

In summary, we demonstrated a controllable and reliable approach to fabricate 10 nm scale nano-gap structures through an elastomeric nano-stamp with an embedded ultra-thin pattern. Unlike other patterning techniques for fabricating a nano-gap structure, our method has several notable advantages. First, the simple fabrication procedure can enable efficient creation of high resolution (approximately 10 nm) nano-gap patterns with complex feature shapes. Second, it can be extended to various other metals and semiconductors, including Pt, Cu and Si. Third, the feature size of the nano-gap structures is easily controlled from 13 nm up to 72 nm using the isotropic RIE process. SERS substrates for detection of single-level molecules were fabricated and demonstrated identical results compared to simulations and previous studies, indicating the potential applications of our technique. This proposed approach can facilitate versatile applications such as molecular electronics, and chemical and biological sensing tools.

Acknowledgements

This research was supported by the National Research Foundation of Korea (NRF-2012R1A2A1A01003537) and the Center for Advanced Soft Electronics under the Global Frontier Research Program (NRF-2012M3A6A5055744) grant funded by the Ministry of Science, ICT and Future Planning, Korea (MSIP). SEM experiments were carried out at NNFC in KAIST.

Notes and references

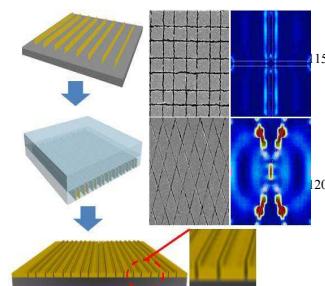
1. Department of Chemical and Biomolecular Engineering, Korea Advanced Institute of Science and Technology, Daejeon, 305-701, Korea. Fax: +82-42-350-3910; Tel: +82-42-350-3931; E-mail: heetae@kaist.ac.kr

[†] These authors contributed equally to this work.

[†] Electronic Supplementary Information (ESI) available: Descriptions of experimental scheme for fabrication of hole-cylinder pattern, See DOI: 10.1039/b000000x/

- 1 T. Li, W. Hu and D. Zhu, *Adv. Mater.*, 2010, **22**, 286-300.
- 2 J. -H. Kim, H. Moon, S. Yoo and Y. -K. Choi, *Small*, 2011, **7**, 2210-2216.
- 3 L. Jiang, H. Dong, Q. Meng, J. Tan, W. Jiang, C. Xu, Z. Wang and W. Hu, *Adv. Mater.*, 2012, **24**, 694-698.
- 4 D. -H. Kim, N. Lu, R. Ghaffari and J. A. Rogers, *NPG Asia Mater.*, 2012, **4**, e15.
- 5 J. R. Health and M. A. Ratner, *Phys. Today*, 2013, **56**, 43-49.
- 6 A. S. Blum, J. G. Kushmerick, D. P. Long, C. H. Patterson, J. C. Henderson, Y. Yao, J. M. Tour, R. Shashidhar and B. R. Ratna, *Nat. Mater.*, 2005, **4**, 167-172.
- 7 H. Park, J. Park, A. K. L. Lim, E. H. Anderson, A. P. Alivisatos and P. L. McEuen, *Nature*, 2000, **407**, 57-60.
- 8 H. -J. Jeon, Y. -K. Baek, S. B. Yang, S. -K. Lee, J. -M. Jung and H. -T. Jung, *J. Mater. Chem.*, 2011, **21**, 14285-14290.
- 9 H. Duan, H. Hu, K. Kumar, Z. Shen and K. W. Yang, *ACS Nano*, 2011, **5**, 7593-7600.
- 10 Y. Wang, X. Liang, Y. Liang and S. Y. Chou, *Nano Lett.*, 2008, **8**, 1986-1990.
- 11 H. Im, K. C. Bantz, N. C. Lindquist, C. L. Haynes and S. -H. Oh, *Nano Lett.*, 2010, **10**, 2231-2236.
- 12 S. Strobel, S. Harrer, G. P. Balnco, G. Scarpa, G. Abstreiter, P. Lugli and M. Tornow, *Small*, 2009, **5**, 579-582.
- 13 S. M. Morton, D. W. Silverstein and L. Jensen, *Chem. Rev.*, 2011, **111**, 3962-3994.
- 14 K. Nakamoto, R. Kurita, O. Niwa, T. Fujii and M. Nishida, *Nanoscale*, 2011, **3**, 5067-5075.
- 15 P. Choi, P. -F. Fu and L. J. Guo, *Adv. Funct. Mater.*, 2007, **17**, 65-70.
- 16 J. Pokki, O. Ergeneman, K. M. Sivaraman, B. Ozkale, M. A. Zeeshan, T. Luhmann, B. J. Nelson and S. Pane, *Nanoscale.*, 2012, **4**, 3083-3088.
- 17 G. Singh, H. J. Griesser, K. Bremmell and P. Kingshott, *Adv. Funct. Mater.*, 2011, **21**, 540-546.
- 18 M. C. Rosamon, A. J. Gallant, M. C. Petty, O. Kolosov and D. A. ZeZe, *Adv. Mater.*, 2011, **23**, 5039-5044.
- 19 M. -S. She, C. Peroz, S. Dhuey, M. Cornet, T. -Y. Lo, H. -Y. Hsueh and R. -M. Ho, *NPG Asia Mater.*, 2013, **5**, e42.
- 20 X. Gu, Z. Liu, I. Gunkel, S. T. Chourou, S. W. Hong, D. L. Olynick and T. P. Russel, *Adv. Mater.*, 2012, **24**, 5688-5694.
- 21 D. J. Lipomi, R. C. Chiehi, M. D. Dickey and G. M. Whitesides, *Nano Lett.*, 2008, **8**, 2100-2105.
- 22 H. -J. Jeon, K. H. Kim, Y. -K. Baek, D. W. Kim and H. -T. Jung, *Nano Lett.*, 2010, **10**, 3604-3610.
- 23 H. S. Jeong, H. -J. Jeon, Y. H. Kim, M. B. Oh, P. Kumar, S. -W. Kang and H. -T. Jung, *NPG Asia Mater.*, 2012, **4**, e7.
- 24 H. -J. Jeon, H. -W. Yoo, E. H. Lee, S. W. Jang, J. -S. Kim, J. K. Choi and H. -T. Jung, *Nanoscale.*, 2013, **5**, 2358-2363.
- 25 A. Plettl, F. Enderle, M. Saitner, A. Manzke, C. Pfahler, S. Wiedemann and P. Ziemann, *Adv. Funct. Mater.*, 2009, **19**, 3279-3284.
- 26 H. Kang, J. Lee, J. Park and H. H. Lee, *Nanotechnology* **2006**, **17**, 197-200.

Table of Contents



125